Locked synchronous rotor motion in a molecular motor

Stacko, Peter; Kistemaker, Jos C. M.; van Leeuwen, Thomas; Chang, Mu-Chieh; Otten, Edwin; Feringa, Ben L.

Published in:
Science

DOI:
10.1126/science.aam8808

Publication date:
2017

MOLECULAR MACHINES

Locked synchronous rotor motion in a molecular motor

Peter Štacko, Jos C. M. Kistemaker, Thomas van Leeuwen, Mu-Chieh Chang, Edwin Otten, Ben L. Feringa*

Biological molecular motors translate their local directional motion into ordered movement of other parts of the system to empower controlled mechanical functions. The design of analogous geared systems that couple motion in a directional manner, which is pivotal for molecular machinery operating at the nanoscale, remains highly challenging. Here, we report a molecular rotary motor that translates light-driven unidirectional rotary motion to controlled movement of a connected biaryl rotor. Achieving coupled motion of the distinct parts of this multicomponent mechanical system required precise control of multiple kinetic barriers for isomerization and synchronous motion, resulting in sliding and rotation during a full rotary cycle, with the motor always facing the same face of the rotor.

Artificial molecular motors (*1*–*5*) have enabled movement at the nanoscale (*6*–*10*) as well as dynamic control of assembly and mechanical, electronic, catalytic, and transport properties (*11*–*20*). Adenosine triphosphatase (ATPase)–mediated transport (*21*), flagella-based bacterial movement (*22*), and protein translocation performed by living organisms are just a few examples demonstrating that transmission and directionality of motion is of fundamental importance for the functioning of biological nanoscale machines. Amplification, propagation, and in particular coupling of the motor movement to other components, which is key to these biological systems, also constitute the basis for geared wheels and sprockets in macroscopic machines, but these complex functions continue to be largely unexplored in molecular systems. Pioneering synthetic studies toward coupled rotors (*23*, *24*) resulted in the cogwheeling motion of two triptycene units arising from complementary steric interactions between tightly fitting rotors (*25*), bevel-gear–shaped rotors based on double-decker porphyrin complexes (*26*), and caterpillar track complexes (*27*). Although they exhibit geared movement, none of these systems display directional behavior controlled and powered by a molecular motor, which is essential to achieving more complex mechanical tasks. Here, we demonstrate controlled rotary and translational motion in a geared system that is driven by a unidirectional rotary motor.

Our design was based on a second-generation molecular motor comprising an upper and lower half connected by a central olefinic bond, which serves as the axle of rotation (Fig. 1A) (*28*). The combination of helical structure, stereogenic center, stilbene type photochemical *E*–*Z* (PEZ) isomerization, and thermal helix inversion (THI) allows unidirectional light-driven rotary motion (*2*). We envisioned that introducing a naphthalene substituent as rotor (Fig. 1A, red) would result in synchronous biaryl motion governed by the photochemically induced unidirectional rotation of the overcrowded alkene. The four-step rotary cycle of the motor, the sliding motion, and conformational changes of the naphthalene rotor are schematically depicted in Fig. 1, B and C. During the 360° rotation of the motor (Fig. 1B, rotation of blue component), one side of the aryl rotor (Fig. 1B, red) continuously faces the lower half (Fig. 1B, black) of the molecular motor, akin to the locked synchronous rotation of the moon, in which only one side of it faces the earth (movies S1 and S2).

To ensure such a synchronous rotation, random thermal biaryl rotation (BR) has to be suppressed by providing a barrier for the BR sufficiently higher than the barrier for thermal helix inversion (THI) of the motor during its rotary process (Fig. 1C). On the other hand, the aryl moiety (Fig. 1C, red) will slide along the lower half of the motor (Fig. 1C, black) in the course of the PEZ isomerization, adjusting the dihedral angle around the biaryl single bond and simultaneously minimizing steric repulsion between itself and the fluorene moiety in the photochemically generated metastable form of the molecular motor (Fig. 1B, step 1). A subsequent THI (Fig. 1B, step 2) proceeds unidirectionally because of the unfavorable pseudoequatorial orientation of the methyl group at the stereogenic center in the indane component of the motor (*28*). As in the photochemical step, the dihedral angle of the biaryl rotor is adjusted, but full BR is blocked (Fig. 1C). Subsequent photochemical (Fig. 1B, step 3) and thermal (Fig. 1B, step 4) steps complete a 360° cycle while the naphthalene rotates around the lower half in a synchronous manner, keeping the same side of the naphthalene unit facing the fluorene part of the motor during the entire rotational cycle.

To achieve locked synchronous motion in such a coupled motor-rotor system, three requirements have to be fulfilled: (i) retention of the absolute stereochemistry (R_a/S_a) of the biaryl bond during the PEZ isomerization and THI steps of the motor unit, both of which feature a (*P*–*M*) helix inversion; (ii) an operating temperature at which the THI takes place at an appreciable rate while the rate of full BR is negligibly low (Fig. 1C); and (iii) sufficient conformational flexibility in the biaryl unit to adjust the dihedral angle during the sliding motions, generating distinct biaryl helical (*P*, *M*) conformations (Fig. 1B). In our design, we expected only the conformation in which the biaryl is parallel to the fluorene because the other conformations with the biaryl oriented perpendicular would induce substantial steric strain (Fig. 1C and supplementary text). The choice of naphthalene as substituent fulfills a final critical design element because it ensures two distinguishable atropisomers. The steric hindrance of the naphthalene rotor is expected to provide a high barrier for BR in structure "B" in Fig. 1C, whereas the methoxy group serves as a simple "brake" moiety to ensure steric hindrance and a concomitant high barrier in structure "D" to prevent BR. On the basis of the combination of all these structural and dynamic features, molecular motor **1** was designed in pursuit of a viable candidate for further theoretical and experimental investigation (Fig. 2).

A computational study was undertaken a priori in order to verify our design, both for stable and metastable motor isomers obtained during the rotary cycle, especially with respect to the delicate balance between the barrier for thermal BR and THI and to establish suitable estimated temperature ranges in which the thermal processes would occur at detectable rates (supplementary text). Several features were revealed in the metastable state of the motor (*S*,*P*,R_a)-**1** with respect to the corresponding stable state [(*S*,*M*,R_a)-**1**]: (i) The helicity of the overcrowded alkene is inverted, (ii) the absolute chirality of the biaryl is preserved, and (iii) the clinal orientation of the naphthalene moiety is inverted [for example, stable-(*S*,*M*,R_a,*synclinal*)-**1** gives metastable-(*S*,*P*,R_a,*anticlinal*)-**1**]. A single transition state connects each local minimum to its corresponding global minimum, during which the naphthalene group slides around the fluorene stator through a 90° torsion angle of the biaryl (inverting syn- or anticlinal conformation). This process allows the overcrowded alkene to invert its helicity and is therefore identified as the THI. The barriers for THI were found to be very low compared with those for BR and would result in predicted half-lives of ~10 min at −50°C, which is a suitable temperature for kinetic analysis. Under these conditions, the lifetime of the stable state (*S*,*P*,R_a)-**1** with respect to atropisomerization of the biaryl moiety is predicted to exceed thousands of years, which renders this undesired BR process completely negligible.

The molecular motor **1** was obtained (supplementary text) as a mixture of two atropisomers in their thermodynamic ratio (3:1) according to ^{1}H nuclear magnetic resonance (NMR) spectroscopy, assigned as (*S**,*M**,R_a*)-**1** and (*S**,*M**,S_a*)-**1** (*29*). Column chromatography followed by three consecutive crystallizations from ethanol afforded the pure major isomer (*S**,*M**,R_a*)-**1** [<5% of

Centre for Systems Chemistry, Stratingh Institute for Chemistry and Zernike Institute for Advanced Materials, Faculty of Mathematics and Natural Sciences, University of Groningen, Nijenborgh 4, Groningen 9747 AG, Netherlands.
*Corresponding author. Email: b.l.feringa@rug.nl

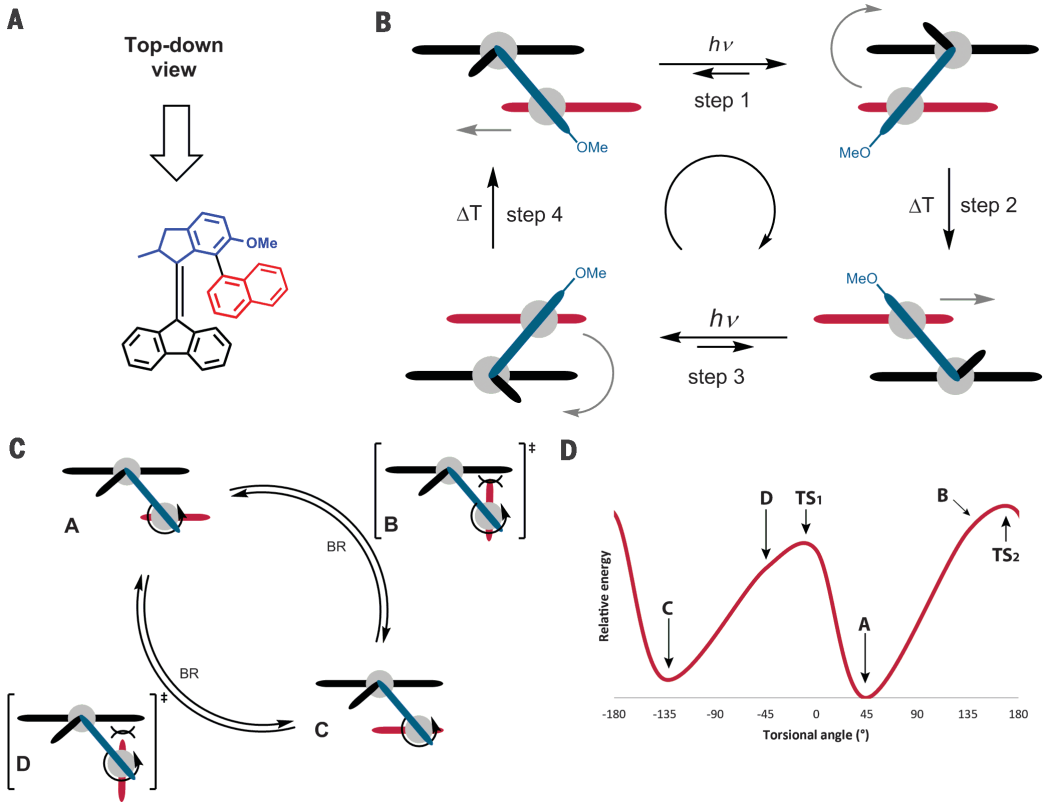

Fig. 1. Design of locked synchronous rotation in a molecular motor. (**A**) Structure of the molecular motor with appending biaryl rotor. Blue, indanyl upper half ; black, fluorene lower half; and red, naphthalene moiety. (**B**) Schematic representation of the photochemically driven rotatory cycle as viewed from the top along the axis given by the double bond. (**C**) Depiction of the four possible conformations of the *R*-substituted biaryl moiety as viewed from the top along the central double bond. (**D**) Energy diagram showing that the two conformers with the naphthalene group perpendicular to the fluorene are disfavored because of steric hindrance.

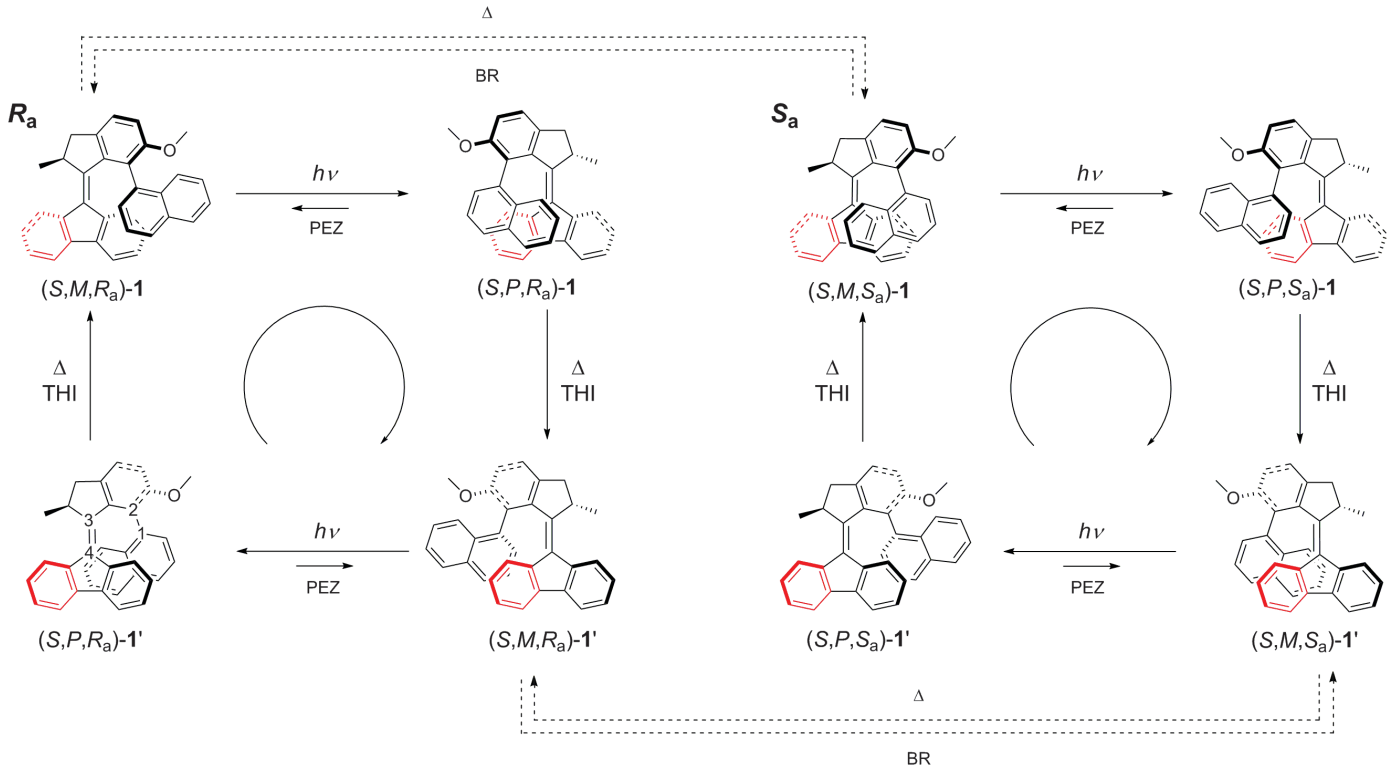

Fig. 2. Rotational cycle of the molecular motor 1. R_a, rotational cycle of (*S*,*M*,R_a)-**1**. The naphthalene moiety slides along the fluorene lower half during the PEZ isomerization [from stable (*S*,*M*,R_a)-**1** to metastable (*S*,*P*,R_a)-**1**], followed by rotation around the fluorene in a synchronous fashion during the THI [from metastable (*S*,*P*,R_a)-**1** to stable (*S*,*M*,R_a)-**1**]. S_a, rotational cycle of (*S*,*M*,S_a)-**1**. The naphthalene moiety slides along the fluorene lower half during the PEZ isomerization [from stable (*S*,*M*,S_a)-**1** to metastable (*S*,*P*,S_a)-**1**], followed by rotation around the fluorene in a synchronous fashion during the THI [from metastable (*S*,*P*,S_a)-**1** to stable (*S*,*M*,S_a)-**1**]. (*S*,*M*,R_a)-**1** and (*S*,*M*,R_a)-**1'** are the same structures, as are (*S*,*M*,S_a)-**1** and (*S*,*M*,S_a)-**1'**. . $t_{½BR} >> t_{½THI}$.

(*S**,*M**,*S*$_a$*)-**1**]. On the basis of the density functional theory calculations, we expected two isomers: one with the naphthyl in a synclinal orientation [(*S**,*M**,*R*$_a$*)-**1**] and another with the naphthyl in an anticlinal orientation [(*S**,*M**,*S*$_a$*)-**1**] (Fig. 2). Comparison of the experimental ^{1}H NMR spectrum of the major isomer and the calculated spectrum [ωB97XD/6-31+G(d,p)//mPW1PW91/6-311+G(2d,p)/SMD=$CHCl_3$] of **1** shows a much stronger correlation with (*S**,*M**,*R*$_a$*)-**1** than with (*S**,*M**,*S*$_a$*)-**1** (supplementary text). This correlation is especially obvious for H^{15} and H^{16}, which experience the ring current of the adjacent naphthalene in the synclinal orientation, shifting the signals upfield to 5.90 and 6.61 parts per million (ppm), respectively (Fig. 3A). The minor isomer exhibits a ^{1}H NMR spectrum without resonances in this characteristic range and is assigned as (*S**,*M**,*S*$_a$*)-**1**. Unequivocal proof of the structure of the major isomer **1** and the synclinal biaryl conformation was based on the x-ray structure of the major isomer (Fig. 3B). The dihedral angle of the biaryl determined from the x-ray analysis was found to be 62.4°, which is in very good agreement with the calculated value of 60.5°. Subsequently, the barrier for BR of (*S**,*M**,*R*$_a$*)-**1** in d_8-toluene was determined by using ^{1}H NMR spectroscopy at elevated temperatures (75 to 95°C) (fig. S23). An Eyring analysis (fig. S24) provided the kinetic parameters [BR enthalpy of activation ($\Delta^{\ddagger}H^{\circ}_{BR}$) 101.1 ± 0.6 kJ mol^{-1}, BR entropy of activation ($\Delta^{\ddagger}S^{\circ}_{BR}$) −33.0 ± 1.6 J K^{-1} mol^{-1}, BR Gibbs free energy of activation ($\Delta^{\ddagger}G^{\circ}_{BR}$) 110.8 ± 0.7 kJ mol^{-1}, and BR half-life ($t_{½BR}$) (363 K) 28.3 ± 0.3 min], which are in good agreement with the calculated values ($\Delta^{\ddagger}G^{\circ}_{BR\text{-}calc}$ = 111.6 kJ mol^{-1}), showing that the half-life for this process at room temperature corresponds to about 75 days.

Irradiation of (*S**,*M**,*R*$_a$*)-**1** in heptane (Fig. 2) with ultraviolet (UV) light (365 nm) at −60°C resulted in the emergence of a bathochromically shifted absorption band in the UV–visible (vis) spectrum that is consistent with the behavior of other second-generation motors and indicative of an increase in alkene strain, as is expected for the metastable form (*S**,*P**,*R*$_a$*)-**1** (Fig. 3C) (*30*). Full reversal to the original UV-vis spectrum was observed at room temperature, indicating that THI was taking place and the rotary motor function was uncompromised (Fig. 3C and supplementary text). Eyring analysis provided the kinetic parameters [$\Delta^{\ddagger}H^{\circ}_{THI}$ 34.5 ± 0.5 kJ mol^{-1}, $\Delta^{\ddagger}S^{\circ}_{THI}$ −143.3 ± 2.3 J K^{-1} mol^{-1}, $\Delta^{\ddagger}G^{\circ}_{THI}$ 76.6 ± 0.8 kJ mol^{-1}, and $t_{½THI}$ (rt) 5.4 ± 1.8 s] (fig. S25), which are in good agreement with those of the calculated barrier [$\Delta^{\ddagger}G_{THI}$ (−50°C) = 66.5 kJ mol^{-1}, $\Delta^{\ddagger}G_{THI\text{-}calc}$ (−50°C) = 65.9 kJ mol^{-1}]. The experimental values of the barriers for both the BR and THI confirmed that the essential condition ($\Delta^{\ddagger}G^{\circ}_{BR}$ >> $\Delta^{\ddagger}G^{\circ}_{THI}$) for synchronous motion had been fulfilled as predicted with calculations.

Irradiation (365 nm, d_8-toluene) of (*S**,*M**,*R*$_a$*)-**1** at −80°C to photostationary state (PSS) produces a new species that lacks ^{1}H NMR resonances at 6.09, 6.53, 8.00, and 7.86 ppm (belonging to H^{15}, H^{16}, H^7, and H^{21}, respectively) and instead exhibits two new resonances at 7.60 and 7.73 ppm (Fig. 3D, ii). These data are consistent with formation of metastable (*S**,*P**,*R*$_a$*)-**1** (38%), in which the naphthalene moiety adopts an anticlinal orientation, thus moving away from the vicinity of the H^{15} and H^{16} (fig. S2). The original ^{1}H NMR spectrum of (*S**,*M**,*R*$_a$*)-**1** is completely recovered upon heating to room temperature, demonstrating that the conformation of the biaryl is indeed fully retained after one-half of the rotational cycle (Fig. 3D, iii). The efficacy of this synchronous motion has been further probed by irradiation (365 nm) of a sample of racemic (*S**,*M**,*R*$_a$/*S*$_a$*)-**1** in CD_2Cl_2 at room temperature for 24 hours. The ratio of (*S**,*M**,*R*$_a$*)-**1** and (*S**,*M**,*S*$_a$*)-**1** remained unchanged in the process, manifesting the efficacy of the process across multiple photochemical cycles (fig. S26). To gain additional insight in the dynamic behavior of the naphthalene rotor moiety, the rotational cycle was followed by means of circular dichroism (CD) spectroscopy (Fig. 4).

For this purpose, a single enantiomer (*R*,*P* or *S*,*M*) of each atropisomer (*R*$_a$ and *S*$_a$) of motor **1** was isolated by using preparative supercritical fluid chromatography (SFC) on a chiral stationary phase [Chiralpak IB (Daicel, Japan), 18% MeOH in CO_2, 3.0 ml min^{-1}, temperature (*T*) = 40°C, 180 bar] (supplementary text).The experimental CD-spectra of the two isolated enantiomers were compared with the calculated spectra, which revealed

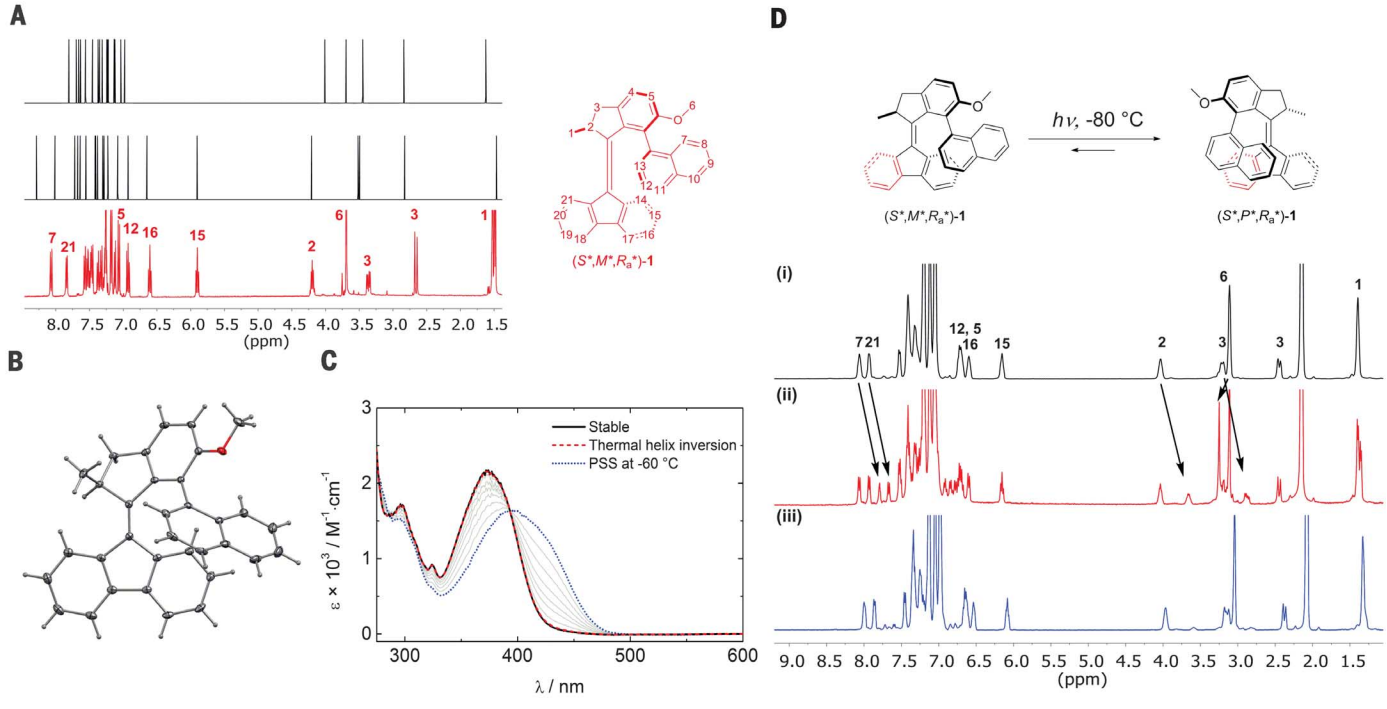

Fig. 3. Characterization of intermediates in the rotation cycle. (**A**) Comparison of the calculated and experimental ^{1}H NMR spectra. (Top) Calculated spectrum of the (*S**,*M**,*S*$_a$*)-**1**. (Middle) Calculated spectrum of the (*S**,*M**,*R*$_a$*)-**1**. (Bottom) ^{1}H NMR ($CDCl_3$, 400 MHz) experimental spectrum of (*S**,*M**,*R*$_a$*)-**1**. A small amount (<4%) of minor (*S**,*M**,*S*$_a$*)-**1** is present. (**B**) X-ray structure of (*S**,*M**,*R*$_a$*)-**1**. (**C**) UV-vis absorption spectrum of (*S**,*M**,*R*$_a$*)-**1** in heptane at −60°C (black solid line); after irradiation (365 nm) to PSS at −60°C (dotted blue line); and after warming to room temperature measured at −60°C (dashed red line). (**D**) (Top) Irradiation of (*S**,*M**,*R*$_a$*)-**1** at −80°C to produce metastable (*S**,*P**,*R*$_a$*)-**1**. (Bottom) ^{1}H NMR spectra (d_8-toluene, 400 MHz, −55°C). (i) (*S**,*M**,*R*$_a$*)-**1** with proton assignments (Fig. 3B) labeled above; (ii) after irradiation (365 nm) at −80°C for 3 hours, appearance of the metastable (*S**,*P**,*R*$_a$*)-**1** denoted by arrows; and (iii) after warming to room temperature for 10 min.

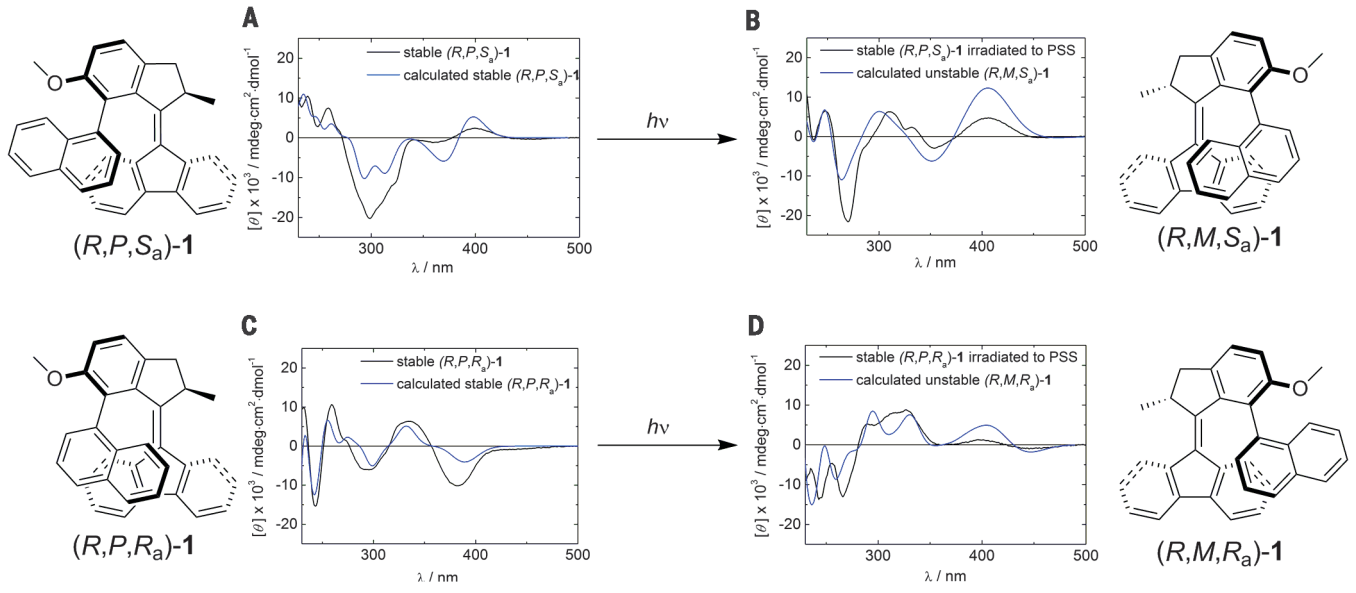

Fig. 4. CD spectra (heptane, −80°C). (**A**) Stable (*R*,*P*,S_a)-**1** (black); calculated stable (*R*,*P*,S_a)-**1** (blue). (**B**) Stable (*R*,*P*,S_a)-**1** irradiated (365 nm) to PSS (black); calculated metastable (*R*,*M*,S_a)-**1** (blue). (**C**) Stable (*R*,*P*,R_a)-**1** (black); calculated stable (*R*,*P*,R_a)-**1** (blue). (**D**) Stable (*R*,*P*,R_a)-**1** irradiated (365 nm) to PSS (black); calculated metastable (*R*,*M*,R_a)-**1**.

a strong correlation with (*R*,*P*,S_a)-**1** in Fig. 4A and with (*R*,*P*,R_a)-**1** in Fig. 4C, providing the absolute stereochemical assignment of the isolated isomers. The experimental CD spectrum of (*R*,*P*,S_a, *synclinal*)-**1** possesses distinct absorption bands with maxima at 299 and 399 nm, whereas the experimental CD spectrum of (*R*,*P*,R_a, *anticlinal*)-**1** shows absorptions bands at 299, 332, and 386 nm (Fig. 4 and supplementary text). Irradiation of separate samples of (*R*,*P*,S_a)-**1** and (*R*,*P*,R_a)-**1** with UV light (365 nm) at −80°C provided the CD spectra of their respective PSS mixtures (Fig. 4, B and D), which exhibit significant changes with respect to their initial configurations. In particular, an overall slight bathochromic shift was observed, which is common for these metastable forms (*30*). The new absorption bands bear resemblance to inverted CD-spectra of the diastereoisomers of their initial stable configurations with opposite axial chirality. For example, the CD-spectrum of the PSS mixture of (*R*,*P*,S_a)-**1** (Fig. 4B) resembles that of a mirror image of (*R*,*P*,R_a)-**1** (Fig. 4C); the exact mirror image of the CD-spectrum of (*R*,*P*,R_a)-**1** belongs to its enantiomer (*S*,*M*,S_a)-**1**. This is to be expected from a synchronously locked rotor system, in which the helicities of the chromophores, which provide the major absorption bands, invert during the PEZ isomerization while retaining their absolute point and axial chirality; for example, stable-(*R*,*P*,S_a)-**1** (Fig. 4A) is expected to photoisomerize to metastable-(*R*,*M*,S_a)-**1** (Fig. 4B), of which the helicities of the chromophores correspond to those of stable-(*S*,*M*,S_a)-**1** (Figs. 2 and 4 and supplementary text).

The formation of (*R*,*M*,S_a)-**1** upon irradiation of (*R*,*P*,S_a)-**1** observed in CD spectra (Fig. 4, A to B) is consistent with the behavior of (*S**,*M**,R_a*)-**1** observed with ^{1}H NMR spectroscopy (Fig. 3D, i and ii), for which the loss of the characteristic signals of H^{15} and H^{16} confirmed movement of the naphthalene orientation from synclinal to anticlinal and thus the formation of (*S**,*P**,R_a*)-**1**. In conjunction, these observations establish that the suggested mode of action—sliding motion of the aryl rotor and helical change in torsion angle—during the PEZ isomerization is taking place. The samples containing the PSS mixtures were then allowed to warm to room temperature, providing CD-spectra identical to those of their respective starting materials (Fig. 4, A and C), in accordance with recovery of the original ^{1}H NMR spectra upon heating (Fig. 3D). These findings unequivocally confirm the proposed mode of rotation for the thermal isomerization (Figs. 1 and 2), during which a second helicity inversion (*M*/*P*) of the motor takes place with retention of the biaryl axial chirality (R_a/S_a). During the THI, the naphthalene group rotates around the fluorene moiety while keeping a single face of the naphthalene faced toward the lower half. This study clearly demonstrates that upon irradiation, the molecular motor exhibits a four-stage unidirectional rotation with concomitant coupled sliding/rotation that keeps the same side of the rotor facing the motor during the entire process.

REFERENCES AND NOTES

1. M. Schliwa, *Molecular Motors* (VCH-Wiley, 2006).
2. W. R. Browne, B. L. Feringa, *Nat. Nanotechnol.* **1**, 25–35 (2006).
3. J. F. Stoddart, *Chem. Soc. Rev.* **38**, 1802–1820 (2009).
4. G. Ragazzon, M. Baroncini, S. Silvi, M. Venturi, A. Credi, *Nat. Nanotechnol.* **10**, 70–75 (2015).
5. L. Greb, J.-M. Lehn, *J. Am. Chem. Soc.* **136**, 13114–13117 (2014).
6. E. R. Kay, D. A. Leigh, F. Zerbetto, *Angew. Chem. Int. Ed.* **46**, 72–191 (2007).
7. J. C. M. Kistemaker, P. Štacko, J. Visser, B. L. Feringa, *Nat. Chem.* **7**, 890–896 (2015).
8. H. Gu, J. Chao, S.-J. Xiao, N. C. Seeman, *Nature* **465**, 202–205 (2010).
9. T. Kudernac *et al.*, *Nature* **479**, 208–211 (2011).
10. T.-G. Cha *et al.*, *Nat. Nanotechnol.* **9**, 39–43 (2014).
11. V. García-López *et al.*, *Nano Lett.* **15**, 8229–8239 (2015).
12. H. L. Tierney *et al.*, *Nat. Nanotechnol.* **6**, 625–629 (2011).
13. M. von Delius, E. M. Geertsema, D. A. Leigh, *Nat. Chem.* **2**, 96–101 (2010).
14. R. A. Bissell, E. Córdova, A. E. Kaifer, J. F. Stoddart, *Nature* **369**, 133–137 (1994).
15. A. Coskun, M. Banaszak, R. D. Astumian, J. F. Stoddart, B. A. Grzybowski, *Chem. Soc. Rev.* **41**, 19–30 (2012).
16. S. Kassem, A. T. L. Lee, D. A. Leigh, A. Markevicius, J. Solà, *Nat. Chem.* **8**, 138–143 (2016).
17. J.-P. Sauvage, *Molecular Machines and Motors (Structure and Bonding)* (Springer-Verlag Berlin Heidelberg, 2001).
18. V. Balzani, A. Credi, M. Venturi, *Molecular Devices and Machines—Concepts and Perspectives for the Nanoworld* (VCH-Wiley, 2008).
19. S. Erbas-Cakmak, D. A. Leigh, C. T. McTernan, A. L. Nussbaumer, *Chem. Rev.* **115**, 10081–10206 (2015).
20. E. R. Kay, D. A. Leigh, *Angew. Chem. Int. Ed.* **54**, 10080–10088 (2015).
21. P. D. Boyer, *Nature* **402**, 247–249, 249 (1999).
22. H. C. Berg, R. A. Anderson, *Nature* **245**, 380–382 (1973).
23. M. Öki, *Angew. Chem. Int. Ed. Engl.* **15**, 87–93 (1976).
24. W. D. Hounshell, C. A. Johnson, A. Guenzi, F. Cozzi, K. Mislow, *Proc. Natl. Acad. Sci. U.S.A.* **77**, 6961–6964 (1980).
25. H. Iwamura, K. Mislow, *Acc. Chem. Res.* **21**, 175–182 (1988).
26. A. Carella, J. Jaud, G. Rapenne, J.-P. Launay, *Chem. Commun. (Camb.)* **19**, 2434–2435 (2003).
27. S. Liu *et al.*, *Angew. Chem. Int. Ed.* **54**, 5355–5359 (2015).
28. N. Koumura, R. W. Zijlstra, R. A. van Delden, N. Harada, B. L. Feringa, *Nature* **401**, 152–155 (1999).
29. The asterisks at the stereodescriptors throughout the text denote a racemic mixture with identical relative stereochemistry: *S**,*M**,S_a* means a mixture of *S*,*M*,S_a and *R*,*P*,R_a.

30. J. Vicario, A. Meetsma, B. L. Feringa, *Chem. Commun. (Camb.)* **47**, 5910–5912 (2005).

ACKNOWLEDGMENTS

This work was supported financially by the Netherlands Organization for Scientific Research (NWO-CW), The Royal Netherlands Academy of Arts and Sciences (KNAW), NanoNextNL of the Government of the Netherlands and 130 partners, the European Research Council (ERC; advanced grant 694345 to B.L.F.), and the Ministry of Education, Culture and Science (Gravitation program 024.001.035). We thank B. S. LeFanu Collins for fruitful discussions and corrections, W. R. Browne for help with low-temperature UV measurements, P. van der Meulen for assistance with low temperature NMR experiments, and E. Smits for help producing the animation. Cambridge Crystallographic Data Centre (CCDC) code CCDC-1540441 contains the supplementary crystallographic data for this paper. These data can be obtained free of charge via www.ccdc.cam.ac.uk/conts/retrieving.html or from the CCDC. Additional data can be found in the supplementary materials and are available from the authors upon request.

SUPPLEMENTARY MATERIALS

www.sciencemag.org/content/356/6341/964/suppl/DC1
Materials and Methods
Supplementary Text
Figs. S1 to S28
Tables S1 to S3
References (*31*–*37*)
Movies S1 and S2

30 January 2017; accepted 21 April 2017
10.1126/science.aam8808

Science

Locked synchronous rotor motion in a molecular motor

Peter Stacko, Jos C. M. Kistemaker, Thomas van Leeuwen, Mu-Chieh Chang, Edwin Otten and Ben L. Feringa

Science **356** (6341), 964-968.
DOI: 10.1126/science.aam8808

Coupled motion in a light-activated rotor

Macroscopic motors rely on gears to keep components in synchrony. Stacko *et al.* demonstrate an analogous type of coupled motion at the molecular scale (see the Perspective by Baroncini and Credi). They constructed a molecular scaffold in which light absorption drives the rotation of upper and lower fragments around a connecting double bond. At the same time, steric constraints modulate the motion of a third component that is tethered to the top of the rotor, so that it continuously exposes the same face to the bottom. The design paves the way toward more complex synchronized motion in an assembly of molecular machines.

Science, this issue p. 964; see also p. 906

Science (print ISSN 0036-8075; online ISSN 1095-9203) is published by the American Association for the Advancement of Science, 1200 New York Avenue NW, Washington, DC 20005. The title *Science* is a registered trademark of AAAS.